Positron Emission Tomography Compartmental Models: A Basis Pursuit Strategy for Kinetic Modelling

Roger N. Gunn[†], Steve R. Gunn[‡], Federico E. Turkheimer[§], John A. D. Aston[†,♯] and Vincent J. Cunningham[§]

[†]McConnell Brain Imaging Center, Montreal Neurological Institute, McGill University, Montreal, Canada

[‡]Image, Speech and Intelligent Systems Group, Dept. of Electronics and Computer Science, University of Southampton, U.K.

[♯]Statistical Research Division, US Census Bureau, Suitland, MD, U.S.A.

[§]Imaging Research Solutions Ltd., Cyclotron Building, Hammersmith Hospital, London, U.K.

November 18, 2002

Abstract

A kinetic modelling approach for the quantification of in vivo tracer studies with dynamic positron emission tomography (PET) is presented. The approach is based on a general compartmental description of the tracer's fate in vivo and determines a parsimonious model consistent with the measured data. The technique involves the determination of a sparse selection of kinetic basis functions from an overcomplete dictionary using the method of basis pursuit denoising. This enables the characterization of the systems impulse response function from which values of the systems macro parameters can be estimated. These parameter estimates can be obtained from a region of interest analysis or as parametric images from a voxel based analysis. In addition, model order estimates are returned which correspond to the number of compartments in the estimated compartmental model. Validation studies evaluate the methods performance against two pre-existing data led techniques, namely graphical analysis and spectral analysis. Application of this technique to measured PET data is demonstrated using [^{11}C]diprenorphine (opiate receptor) and [^{11}C]WAY-100635 (5-HT$_{1A}$ receptor). Whilst, the method is presented in the context of PET neuroreceptor binding studies, it has general applicability to the quantification of PET/SPET radiotracer studies in neurology, oncology and cardiology.

Keywords: *PET, Tracer Kinetics, Compartmental Modelling, Parameter Estimation, Basis Pursuit Denoising, Sparse Basis Selection*

1 Introduction

The development of Positron Emission Tomography (PET) over the last two decades has provided neuroscientists with a unique tool for investigating the neurochemistry of the human brain *in vivo*. The ever increasing library of radiolabelled tracers allows for imaging of a range of biochemical, physiological and pharmacological processes. Each radiotracer has its own distinct behavior *in vivo* and their characterization is an essential component for the development of new imaging techniques and their translation into clinical applications. Estimation of quantitative biological images from the rich 4D spatio-temporal data sets requires the application of appropriate tomographic reconstruction and tracer kinetic modelling techniques. The latter are used to estimate biological parameters by fitting a mathematical model to the time-activity curve (TAC) of a region of interest or voxel. Calculations at the voxel level produce parametric images but are associated with an increase in noise for the TACs. Analysis strategies must therefore be robust to noise, yet fast enough to be practical.

There are a range of quantitative PET tracer kinetic modelling techniques which return biologically based parameter estimates. These techniques may be broadly divided into *model-driven* methods (Kety, 1951; Sokoloff et al., 1977; Phelps et al., 1979; Mintun et al., 1984; Huang and Phelps, 1986; Gunn et al., 2001) and *data-driven* methods (Gjedde, 1982; Patlak et al., 1983; Patlak and Blasberg, 1985; Logan et al., 1990, 1996; Cunningham and Jones, 1993). The clear distinction is that the *data-driven* methods require no *a priori* decision about the most appropriate model structure. Instead this information is obtained directly from the kinetic data.

Model-driven methods use a particular compartmental structure to describe the behaviour of the tracer and allow for an estimation of either micro or macro system parameters. Well established compartmental models in PET, (see Figure 1), include those used for the quantification of blood flow (Kety, 1951), cerebral metabolic rate for glucose (Sokoloff et al., 1977) and for neuroreceptor ligand binding (Mintun et al., 1984). Further developments have produced a series of reference tissue models which avoid the need for blood sampling (Blomqvist et al., 1989; Cunningham et al., 1991; Hume et al., 1992; Lammertsma et al., 1996; Lammertsma and Hume, 1996; Watabe et al., 2000). Parameter estimates are obtained from *a priori* specified compartmental structures using one of a variety of least squares fitting procedures; linear least squares (Carson, 1986), non-linear least squares (Carson, 1986), generalized linear least squares (Feng et al., 1996), weighted integration (Carson et al., 1986) or basis function techniques (Koeppe et al., 1985; Cunningham and Jones, 1993; Gunn et al., 1997). *Data-driven* methods such as graphical analysis (Gjedde, 1982; Patlak et al., 1983; Patlak and Blasberg, 1985; Logan et al., 1990, 1996) or spectral analysis (Cunningham and Jones, 1993) derive macro system parameters from a less constrained description of the kinetic processes. The graphical methods (Patlak and Logan plots) employ a transformation of the data such that a linear regression of the transformed data yields the macro system parameter of interest and are attractive and elegant due to their simplicity. However, they require the determination of when the plot becomes linear, they may be biased by statistical noise (Slifstein and Laruelle, 2000) and they fail to return any information about the underlying compartmental structure. Appendix A gives a formal derivation of the Logan plot and shows that it is valid for an arbitrary number of compartments for both plasma and reference input models when the data are free from noise. Spectral analysis (Cunningham and Jones, 1993) characterizes the systems impulse response function (IRF) as a positive sum of exponentials and uses non-negative least squares to fit a set of these basis functions to the data. The macro system parameters of interest are then calculated as functions of the IRF (Cunningham and Jones, 1993; Gunn et al., 2001). Spectral analysis also returns information on the number of tissue compartments evident in the data and is defined as a *transparent* technique. Schmidt (1999) showed that for the majority of plasma input models the observation of all compartments led to only positive coefficients, and as such the spectral analysis (Cunningham and Jones, 1993) solution using non-negative least squares is valid.

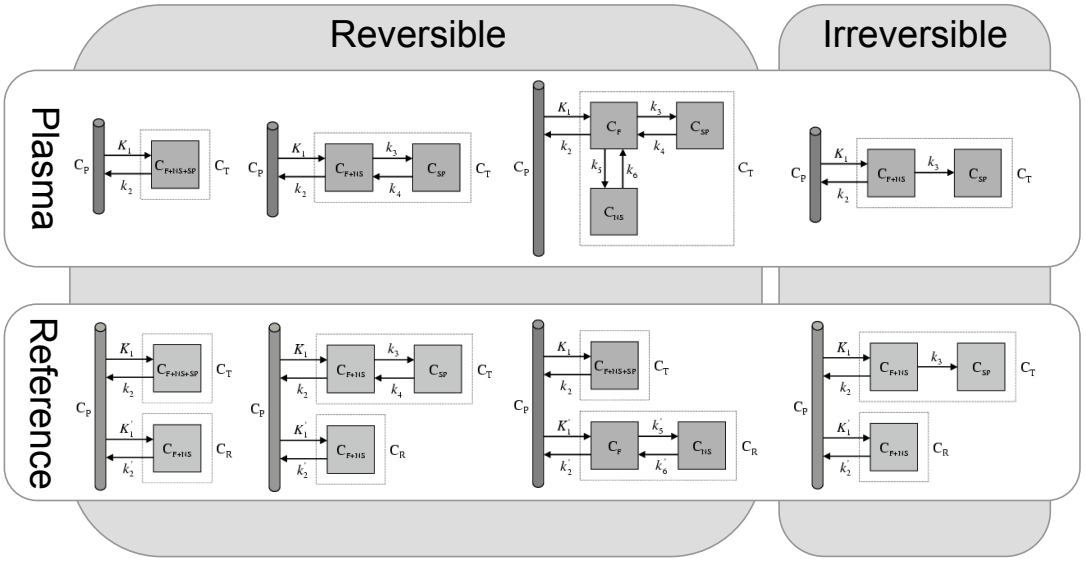

FIGURE 1: A range of PET compartmental models commonly used to quantify PET radiotracers. These include models for tracers that exhibit reversible and irreversible kinetics and models which use either a plasma or reference tissue input function.

However, it is straightforward to deduce that for reference tissue input models negative coefficients can be encountered and that this approach is strictly not valid (see Appendix C in Gunn et al. (2001)).

Recently, we have published general theory for both plasma input and reference tissue input models (Gunn et al., 2001). This work shows that a general PET tracer compartmental system may be characterized in terms of its impulse response function (IRF), and that this is independent of the administration of the tracer and is therefore applicable to both bolus and bolus-infusion methodologies. The term tracer excludes multiple injection protocols involving low specific activity injections which are classed as non-tracer studies and lead to non-linear compartmental systems. In brief, a general PET tracer compartmental model leads to a set of first order linear differential equations. This set of equations may be solved to yield an expression for the total tissue radioactivity concentration in terms of either a plasma input function or a suitable reference tissue input function. These results are derived from linear systems theory which lead to the deduction that the IRF is comprised solely of exponentials and a delta function (Gunn et al., 2001). This work forms the foundation for the presented method; Data-driven estimation of parametric images based on compartmental theory (DEPICT).

DEPICT allows for the estimation of parametric images or regional parameter values from dynamic PET data. DEPICT requires no *a priori* description of the tracers fate *in vivo*, it derives the model description from the data and it returns the number of compartments (model order). This *transparent* modelling technique has application to a wide range of PET radiotracers but the emphasis here is with respect to the analysis of radioligands which bind to specific neuroreceptor sites.

2 Theory

This section introduces the theory behind DEPICT; Firstly, the general forms for plasma input and reference tissue input models are presented, secondly, key parameters for neuroreceptor binding studies are cast in this framework, and thirdly, the general parameter estimation approach is constructed using

basis functions and solved via basis pursuit denoising. The method encompasses the majority of linear compartmental systems which are applicable to tracer studies with an arbitrary input function. It assumes that there is only one form (the parent compound) in which radioactivity enters the tissue from the arterial plasma. Specifically, those models which are defined by Definitions 1 and 2 in Gunn et al. (2001) are considered. These sets of models encompass all non-cyclic systems, the subset of cyclic systems in which the product of rate constants is the same regardless of direction for every cycle and requires the eigenvalues of the system to be distinct.

2.1 Plasma Input Models

The general equation for a plasma input compartmental model is given by,

$$C_T(t) = V_B\, C_B(t) + (1 - V_B) \sum_{i=1}^{n} \phi_i e^{-\theta_i t} \otimes C_P(t). \tag{1}$$

where n is the total number of tissue compartments in the target tissue, $\otimes$ is the convolution operator, V_B is the fractional blood volume, C_T,C_P, and C_B are the concentration time courses in the target tissue, plasma and whole blood respectively. The delivery of the tracer to the tissue is given by $K_1 = \sum_{i=1}^{n} \phi_i$.

Reversible Kinetics $[\theta_i > 0]$

For compartmental models which exhibit reversible kinetics the volume of distribution, V_D, which is equal to the integral of the impulse response function is given by,

$$V_D = \sum_{i=1}^{n} \frac{\phi_i}{\theta_i}. \tag{2}$$

Irreversible Kinetics $[\theta_{i\neq n} > 0, \theta_n = 0]$

For compartmental models which exhibit irreversible kinetics the net irreversible uptake rate constant from plasma, K_I, is given by,

$$K_I = \phi_n. \tag{3}$$

2.2 Reference Tissue Input Models

The general equation for a reference tissue input compartmental model is given by,

$$C_T(t) = \phi_0\, C_R(t) + \sum_{i=1}^{m+n-1} \phi_i e^{-\theta_i t} \otimes C_R(t). \tag{4}$$

where m is the total number of tissue compartments in the reference tissue, and n is the total number of tissue compartments in the target tissue, C_T and C_R are the concentration time courses in the target and reference tissues respectively and R_I $(= \phi_0)$ is the ratio of delivery of the tracer between

the target and reference tissue. This definition excludes the presence of blood volume components to either of the tissues. Explicit formulation including a blood volume term has been given previously (Gunn et al., 2001).

Reversible Target Tissue Kinetics $[\theta_i > 0]$

For reference tissue models which exhibit reversible kinetics in both the target and reference tissues the volume of distribution ratio is given by the integral of the impulse response of the system,

$$\frac{V_D}{V'_D} = \phi_0 + \sum_{i=1}^{m+n-1} \frac{\phi_i}{\theta_i}. \tag{5}$$

Irreversible Target Tissue Kinetics $[\theta_{i\neq m+n-1} > 0, \theta_{m+n-1} = 0]$

For reference tissue models which exhibit irreversible kinetics in the target tissue and reversible kinetics in the reference tissue the normalised irreversible uptake rate constant from plasma is given by,

$$\frac{K_I}{V'_D} = \phi_{m+n-1}. \tag{6}$$

2.3 Parameters for Neuroreceptor Binding Studies

For reversible neuroreceptor binding studies the binding potential may be calculated from the macro parameters, using either a plasma or reference tissue input function, under the assumption that the volume of distribution of the free and non-specific binding is the same in the target and reference tissues. Throughout this paper the term binding potential is used interchangeably to refer to BP (the binding potential as originally defined by Mintun et al. (1984)), $BP.f_2$ and $BP.f_1$ where f_2 and f_1 are the tissue and plasma free fractions respectively. For a reference tissue input analysis $BP.f_2$ is the only binding potential estimate possible, whilst with a plasma input analysis it is possible to obtain estimates for $BP.f_1$, $BP.f_2$ and if a separate measure of the plasma free fraction exists BP. The binding potential is a useful measure of receptor specific parameters which includes the both the maximum concentration of receptor sites and the affinity,

$$BP = \frac{B_{max}}{K_{D_{Tracer}}(1 + \sum_i \frac{F_i}{K_{D_i}})}, \tag{7}$$

where B_{max} is the maximum concentration of receptor sites, $K_{D_{Tracer}}$ is the equilibrium disassociation rate constant of the radioligand, F_i and K_{D_i} are the free concentration and equilibrium disassociation constants of i competing ligands. To derive values for both the receptor concentration and affinity it is necessary to perform a multi-injection study with differing specific activities of the the radioligand. A summary of commonly used receptor binding parameters and their calculation from the general form of the IRF are given in Table 1, for further details see (Gunn et al., 2001). The relative merits of these different binding parameters are discussed elsewhere (Laruelle, 2000).

Parameter	Target	Reference	Input	Calculation
V_D	$\mathcal{R}$	–	C_P	$\sum_{i=1}^{n} \frac{\phi_i}{\theta_i}$
K_I	$\mathcal{I}$	–	C_P	ϕ_n
$BP.f_1$	$\mathcal{R}$	$\mathcal{R}$	C_P	$\sum_{i=1}^{n} \frac{\phi_i}{\theta_i} - \sum_{i=1}^{m} \frac{\varphi_i}{\vartheta_i}$
$BP.f_2$	$\mathcal{R}$	$\mathcal{R}$	C_P	$\frac{\sum_{i=1}^{n} \frac{\phi_i}{\theta_i}}{\sum_{i=1}^{m} \frac{\varphi_i}{\vartheta_i}} - 1$
$BP.f_2$	$\mathcal{R}$	$\mathcal{R}$	C_R	$\phi_0 - 1 + \sum_{i=1}^{m+n-1} \frac{\phi_i}{\theta_i}$
$\frac{K_I}{V_D}$	$\mathcal{I}$	$\mathcal{R}$	C_R	ϕ_{m+n-1}

TABLE 1: Calculation of commonly used binding parameters from the general impulse response function. ϕ and θ are the parameters for the target tissue, φ and ϑ are the parameters for the reference tissue and $\mathcal{R}$ and $\mathcal{I}$ denote reversible and irreversible tissue kinetics respectively.

2.4 Construction of the General Model in a Basis Function Framework

Plasma input[1] and reference tissue input PET compartmental models are characterized by,

$$C_T(t) = \left[\phi_0\delta(t) + \sum_{i=1}^{q} \phi_i e^{-\theta_i t}\right] \otimes C_I(t). \tag{8}$$

where C_T is the tissue concentration time course and C_I is the concentration time course of the input function (plasma or reference tissue). This can be expressed as an expansion on a basis,

$$C_T(t) = \sum_{i=0}^{N} \phi_i \psi_i(t), \tag{9}$$

where

$$\psi_0(t) = C_I(t), \tag{10}$$

$$\psi_i(t) = \int_0^t e^{-\theta_i(t-\tau)} C_I(\tau) d\tau. \tag{11}$$

A set of N values for θ_i may be pre-chosen from a physiologically plausible range $\theta_{min} \leq \theta_i \leq \theta_{max}$. Here, the θ_i values are spaced in a logarithmic manner to elicit a suitable coverage of the kinetic spectrum. Other possibilities for the spacing of the basis exist such as an equi-angular scheme (Cunningham et al., 1998). For data that has not been corrected for the decay of the isotope θ_{min} may be chosen as (or close to the decay constant ($\theta_{min} = \lambda$ min^{-1}) for the radioisotope and θ_{max} may be chosen as a suitably large value ($\theta_{max} = 6$ min^{-1}). For reversible systems, where the calculation of V_D or $BP.f_2$ is the goal, the choice of a value for θ_{min} which is slightly bigger than λ can suppress the calculation of infinite V_D and $BP.f_2$ values from noisy data. PET measurements are acquired as a sequence of (F) temporal frames. Thus, the continuous functions must be integrated over the individual frames and normalized to the frame length to correspond to the data sampling procedure.

[1]Here, the blood volume term for plasma input models is treated as a plasma volume term (i.e. $C_B(t) = C_P(t)$) which enables us to express both the plasma and reference tissue input cases in the same framework. This is simply so that we may be concise in our notation. To use a whole blood volume term $\psi_0 = C_P$ is replaced by $\psi_0 = C_B$ in equation (10).

The tissue observations, $\mathbf{y}$, already exist in this form and correspond to,

$$\begin{aligned} \mathbf{y} &= [y_1 \ \dots \ y_F]^T, \\ y_j &= \frac{1}{t_j^e - t_j^s} \int_{t_j^s}^{t_j^e} C_T(t)dt, \end{aligned} \tag{12}$$

and the matrix of kinetic basis functions (or dictionary), $\mathbf{\Psi}$, are pre-calculated as,

$$\begin{aligned} \mathbf{\Psi} &= \begin{pmatrix} \psi_{01} & \psi_{11} & \dots & \psi_{N1} \\ \vdots & \vdots & \vdots & \vdots \\ \psi_{0F} & \psi_{1F} & \dots & \psi_{NF} \end{pmatrix}, \\ \psi_{0j} &= \frac{1}{t_j^e - t_j^s} \int_{t_j^s}^{t_j^e} C_I(t)dt, \\ \psi_{ij} &= \frac{1}{t_j^e - t_j^s} \int_{t_j^s}^{t_j^e} \int_0^t e^{-\theta_i(t-\tau)} C_I(\tau)d\tau dt, \end{aligned} \tag{13}$$

where t_j^s and t_j^e are the sequences of start and end frame times ($j = 1, \dots, F$). For all practical purposes (i.e. choosing a large enough value for N to obtain a good coverage of the kinetic spectrum), this leads to an overcomplete basis ($N > F - 1$) which by definition is non-orthogonal. Examples bases for a plasma and reference tissue input are displayed in Figure 2. To determine the fit to the data it is necessary to solve the underdetermined system of equations,

$$\mathbf{y} \cong \mathbf{\Psi}\boldsymbol{\phi}. \tag{14}$$

To account for the temporally varying statistical uncertainty of the measurements it is more appropriate to consider the weighted least squares problem,

$$\mathbf{W}^{\frac{1}{2}}\mathbf{y} \cong \mathbf{W}^{\frac{1}{2}}\mathbf{\Psi}\boldsymbol{\phi}, \tag{15}$$

where $\mathbf{W}$ is the inverse of the covariance matrix. Given the statistical independence of the frames, $\mathbf{W}$ is diagonal. These diagonal elements can be approximated from the total image TAC and frame durations (Mazoyer et al., 1986). The weighted least squares solution is simply obtained by weighting both the data and the basis functions i.e. $\mathbf{y}$ is replaced by $\mathbf{W}^{\frac{1}{2}}\mathbf{y}$ and $\mathbf{\Psi}$ is replaced by $\mathbf{W}^{\frac{1}{2}}\mathbf{\Psi}$. On solution of this equation the appropriate macro parameters (V_D, K_I, K_1, $\frac{V_D}{V_D'}$, $\frac{K_I}{V_D'}$, R_I) may be calculated from the $\boldsymbol{\phi}$'s (see equations 2,3,5, and 6). If the data are not corrected for the decay of the isotope, then λ should first be subtracted from the θ values..

2.5 Solution of the General Model by Basis Pursuit Denoising

Standard least squares techniques are not applicable because of the overcomplete basis which leads to an under-determined set of equations. This ill-posed problem requires an additional constraint to impose a unique solution on the estimation process. This constraint is chosen to be consistent with prior knowledge about the solution; namely that the solution will be sparse in the basis coefficients. This constraint has also been used in the wavelet community, for the estimation of sparse representations from over-complete dictionaries (Chen, 1995; Chen et al., 1999). The motivation for sparseness is consistent with the expectation that the data is accurately described by a few compartments (such

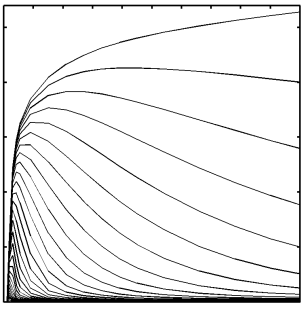

(a) Plasma input basis

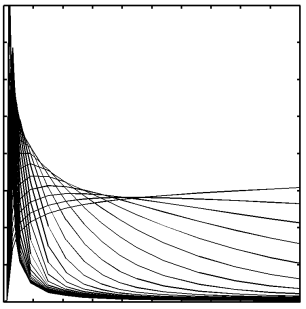

(b) Normalised plasma input basis

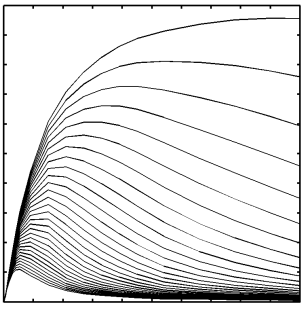

(c) Reference tissue input basis

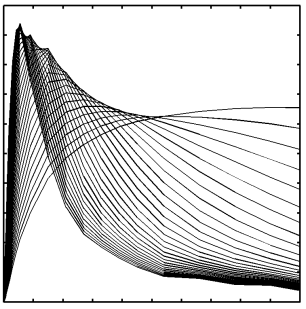

(d) Normalised reference tissue input basis

FIGURE 2: Example Dictionaries ($\boldsymbol{\Psi}$)

as the models in Figure 1).

To transform the problem so that a unique solution exists it is necessary to change the metric from ordinary least squares. The introduction of a regularizer or penalty function to the standard least squares metric offers a framework for this,

$$\min_{\phi} \frac{1}{2} \left\| \mathbf{W}^{\frac{1}{2}} \left(\mathbf{y} - \boldsymbol{\Psi} \boldsymbol{\phi} \right) \right\|_2^2 + \mu \left\| \boldsymbol{\phi} \right\|_p, \tag{16}$$

where the regularization parameter $\mu(> 0)$ controls the trade-off between approximation error and sparseness, $\boldsymbol{\Psi}$ is the overcomplete basis, $\boldsymbol{\phi}$ are the basis coefficients to be determined and $\mathbf{y}$ is the observed data. The addition of an L_p norm to the standard L_2 norm in equation 16 allows for a uniquely determined parameter estimation process. Some possible choices for L_p are L_0 (atomic decomposition), L_1 (basis pursuit de-noising), and L_2 (ridge regression) (Chen, 1995). The three regularisers have different characteristics and implementations. Both atomic decomposition and basis pursuit de-noising promote a sparse solution which is consistent with our expectation of a compartmental model consisting of just a few tissue compartments, whilst ridge regression will encourage all parameters to be non-zero. Atomic decomposition is computationally demanding due to its combinatorial nature. Both basis pursuit de-noising and ridge regression can be constructed in a quadratic programming framework. Given these factors, a good choice for the estimation process is basis pursuit denoising as this balances both a sparse solution with a computationally feasible parameter estimation approach.

The basis pursuit denoising solution to the problem is presented here,

$$\min_{\phi} \frac{1}{2} \left\| \mathbf{W}^{\frac{1}{2}} \left(\mathbf{y} - \mathbf{\Psi}\boldsymbol{\phi} \right) \right\|_2^2 + \mu \left\| \boldsymbol{\phi} \right\|_1, \tag{17}$$

With the introduction of slack variables basis pursuit de-noising can be written as a simple bound constrained quadratic program, (Chen, 1995; Chen et al., 1999),

$$\min_{\boldsymbol{x}} \frac{1}{2} \boldsymbol{x}^T \mathbf{H} \boldsymbol{x} + \mathbf{c}^T \boldsymbol{x}, \tag{18}$$

such that $x_i \geq 0$ and where,

$$\mathbf{H} = \begin{bmatrix} \mathbf{\Psi}^T \mathbf{W} \mathbf{\Psi} & -\mathbf{\Psi}^T \mathbf{W} \mathbf{\Psi} \\ -\mathbf{\Psi}^T \mathbf{W} \mathbf{\Psi} & \mathbf{\Psi}^T \mathbf{W} \mathbf{\Psi} \end{bmatrix}, \tag{19}$$

$$\mathbf{c} = \mu \mathbf{1} - \begin{bmatrix} \mathbf{\Psi}^T \mathbf{W} \mathbf{y} \\ -\mathbf{\Psi}^T \mathbf{W} \mathbf{y} \end{bmatrix}, \tag{20}$$

$$\boldsymbol{x} = \begin{bmatrix} \boldsymbol{\phi}^+ \\ \boldsymbol{\phi}^- \end{bmatrix}. \tag{21}$$

The basis coefficients are given by,

$$\boldsymbol{\phi} = \boldsymbol{\phi}^+ - \boldsymbol{\phi}^-. \tag{22}$$

The quadratic program can be solved readily using standard optimisers (Mészáros, 1998). Thus, given a suitable regularization parameter, the general compartmental model can be fitted to the data. A method which enables the selection of an appropriate regularization parameter is now considered.

Selection of the Regularization Parameter (μ)

Basis pursuit denoising requires the determination of the regularization parameter, μ, for the penalty term. Here, this is obtained by the method of leave one out cross-validation (LOOCV) (Shao, 1993; Hjorth, 1994). LOOCV is a "resampling" method which allows the generalisation error to be estimated. Fits are performed in which each data point is omitted in turn, and the generalisation error is then estimated by summing up the prediction error for each omitted data point. The regularization parameter, μ, is chosen to minimize this estimate (see Figure 3). To achieve a more robust estimate of the most appropriate μ value LOOCV is applied to a set of time activity curves and the mean μ value is selected.

Model Order and Transparency

The presented method is transparent because it returns information about the underlying compartmental structure. The number of non-zero coefficients returned corresponds to the *model order* which is related to the number of tissue compartments. The number of non-zero components is counted as the number of distinct peaks within the spectrum. The method will often include two peaks next to each other in order to approximate an exponential in between them. This occurrence is treated as a single non-zero coefficient. For plasma input models the *model order* equals the number of tissue compartments (ignoring the blood volume component) and for reference tissue models the number of non-zero coefficients corresponds to the total number of tissue compartments in the reference and target tissues.

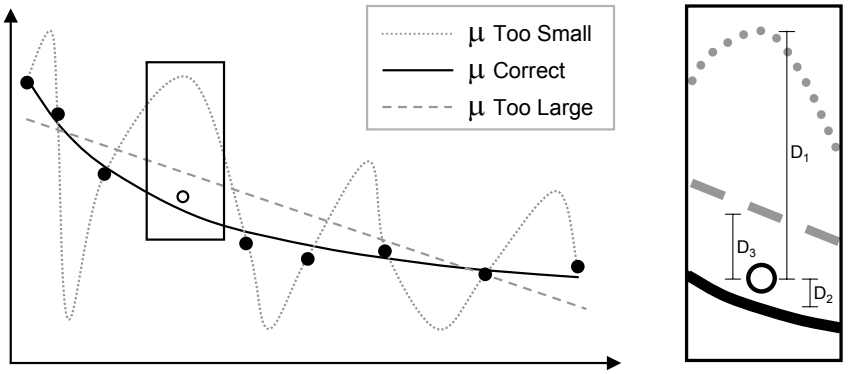

FIGURE 3: Effect of the regularization parameter (μ) and selection via leave one out cross validation: When the μ value is too small the data ($\bullet$) are overfitted and when the value is too big the data are underfitted. The "best" μ value is chosen using LOOCV. A data point is omitted ($\circ$) and the data are fit for a set of μ values. The error in the models prediction of the omitted data point is then calculated in a least squares sense (i.e. D_i^2). This is repeated for the omission of each data point in turn and the resultant generalisation errors are summated. A μ is selected by choosing the value of μ which minimises this generalisation error. The figure shows how the parsimonious model minimises the generalisation error (i.e. $D_2^2 < D_3^2 < D_1^2$).

Whilst, the model order dictates the number of compartments, any decision about the true model configuration is limited by the problem of indistinguishability. Figures 4 and 5 depict the sets of models which are equivalent in terms of model order for plasma input and reference tissue input models. If one requires a compartmental description of the tracer, and the set is not singular, then it is necessary to invoke biological information about the system in order to select amongst the possible models.

3 Methods

For DEPICT and spectral analysis the tissue and plasma data were uncorrected for the decay of the isotope. Instead, a decay constant was allowed for in the exponential coefficients (decay constant for [^{11}C]: $\lambda = 0.034$ min^{-1}). For the Logan analysis the tissue and plasma data were pre-corrected for the decay of the isotope.

DEPICT

The Basis Pursuit denoising approach was implemented with 30 basis functions (logarithmically spaced between 0.048 and 6 min^{-1}). The number of basis functions was chosen to be 30 based on a balance between precision and computation time (data not shown). The weighting matrix was determined from the true TAC activity and the frame duration as described previously (Gunn et al., 1997). The regularization parameter, μ, was determined by numerically minimising the LOOCV error across a discrete set of logarithmically spaced μ values ($10^{-3.5} \leq \mu \leq 10^{0.5}$). For the 1D simulations, the parameter $\hat{\mu}$ was determined as the mean value from the 1000 realisations. For parametric imaging the $\hat{\mu}$ value was obtained from a series of LOOCV estimates (μ_i) obtained from random voxel locations contained within a brain mask. This process examined at least 20 voxels and continued until the

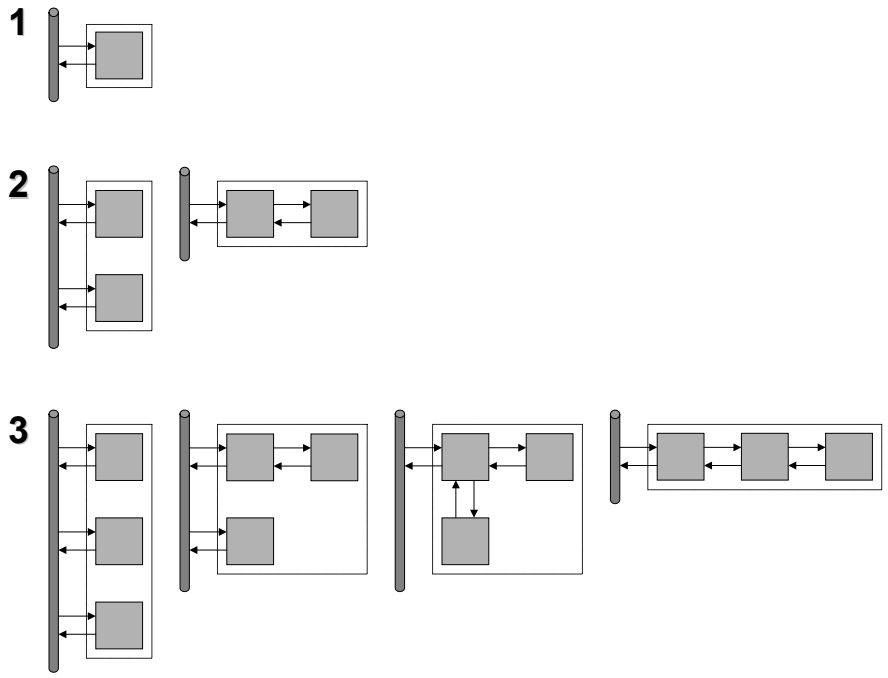

FIGURE 4: Indistinguishability for plasma input models. (top) Model Order=1: One possible configuration, (middle) Model Order=2: Two possible configurations, (bottom) Model Order=3: Four possible configurations.

relative precision of $\hat{\mu}$ was less than 50%,

$$\frac{t_{0.975,df}\sigma(\boldsymbol{\mu})}{\sqrt{N}\ \overline{\boldsymbol{\mu}}} < 0.5, \tag{23}$$

where *df* is the degrees of freedom and is given by the length of $\boldsymbol{\mu} - 1$. $\hat{\mu}$ was then estimated as the mean of the vector $\boldsymbol{\mu}$. DEPICT is available at http://www.bic.mni.mcgill/r̃gunn.

Spectral Analysis

Spectral analysis was implemented using the non-negative least squares algorithm (Cunningham and Jones, 1993) with the identical basis and weighting matrix as were used for DEPICT.

Logan Analysis

The Logan analysis (Logan et al., 1990, 1996) was implemented as a linear regression of the transformed data after 45 minutes.

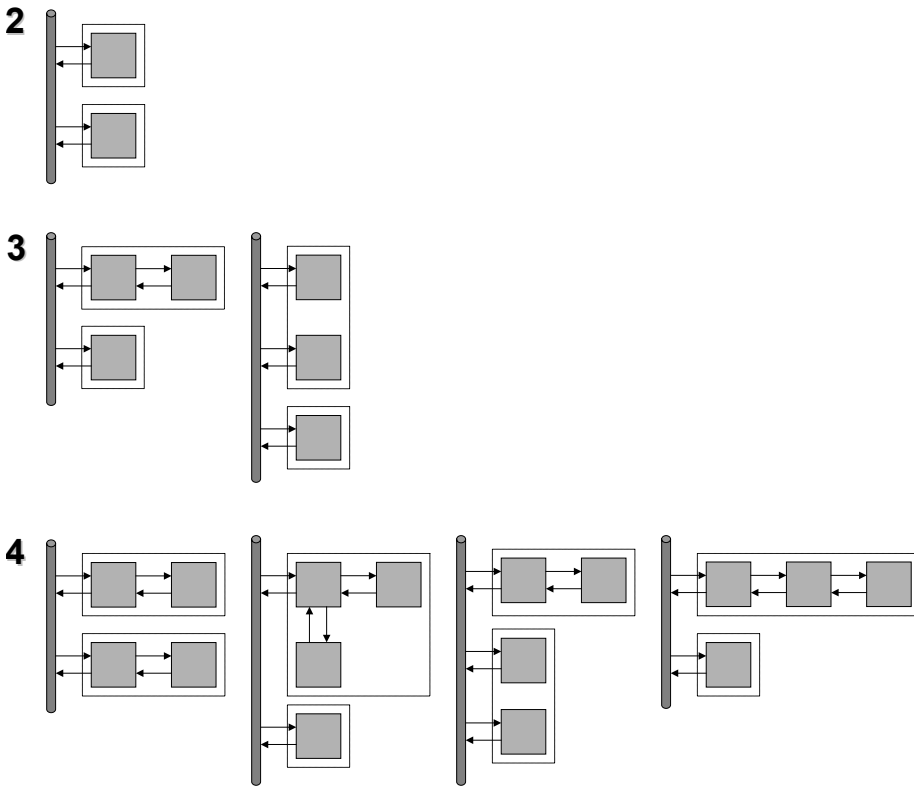

FIGURE 5: Indistinguishability for reference tissue input models. (top) Model Order=2: One possible configuration, (middle) Model Order=3: Four* possible configurations, (bottom) Model Order=4: Eight* possible configurations. *There are twice as many possible configurations than are shown, as the reference and target tissues may be reversed.

3.1 1D Simulations

Simulations were performed to assess the stability of the three methods to different noise levels. A measured input function from a PET scan was used in conjunction with a two tissue compartmental model to simulate noise free data representative of a target tissue ($K_1 = 0.4$ (mL plasma).(mL tissue)$^{-1}$, $k_2 = 0.2$ min^{-1}, $k_3 = 0.4$ min^{-1} and $k_4 = 0.1$ min^{-1}) and a reference tissue ($K_1' = 0.4$ (mL plasma).(mL tissue)$^{-1}$, $k_2' = 0.4$ min^{-1}, $k_5' = 1$ min^{-1} and $k_6' = 1$ min^{-1}). 90 minutes of data were simulated for a total of 24 temporal frames (3x10s, 3x20s, 3x60s, 5x120s, 5x300s, 5x600s). The noise free simulated data are shown in Figure 6. For a range of noise levels 1000 realisations of noisy target tissue TAC's were generated by adding normally distributed noise proportional to the activity/frame duration at each point. The noise variance was scaled so that a value of 1 corresponded to the largest noise free TAC value. These data were then analyzed in two different ways; 1) using the plasma input function the noisy target tissue TAC's were fitted with the basis pursuit method, the Logan plot and spectral analysis to derive V_D estimates, 2) using the reference tissue input function the noisy target tissue TAC's were fitted with the basis pursuit method and the Logan plot to derive $BP.f_2$ estimates.

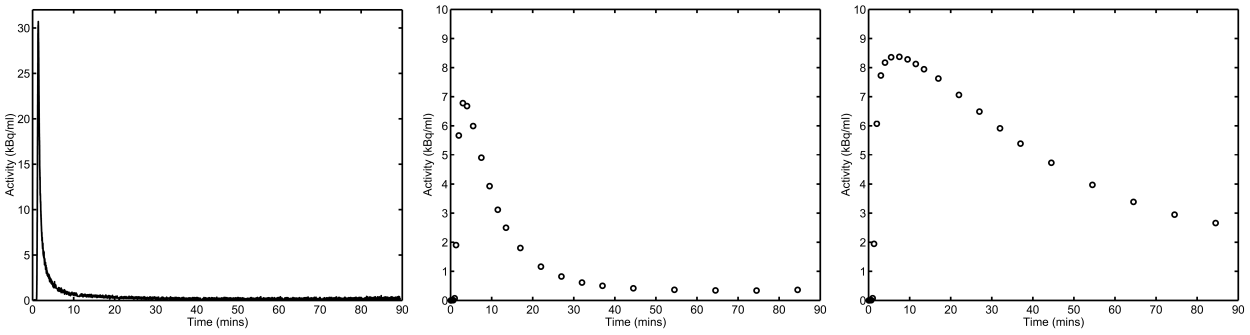

(a) Plasma input function (b) Reference tissue TAC (c) Target tissue TAC

FIGURE 6: 1D Simulation Data: Noise free time activity curves

3.2 4D Simulations

Simulated dynamic PET data were generated using PETSim, a dynamic PET simulator (Ma et al., 1993; Ma and Evans, 1997) as described previously (Aston et al., 2000). In short, the simulator takes an MRI image volume segmented into 28 regions, each of which is assigned an activity value, and generates a simulated PET volume. The resolution and noise characteristics where chosen to correspond to the ECAT HR+ PET camera (CTI, Knoxville, TN) in 3-D mode with a resolution of 4 x 4 x 4.2 mm FWHM at the center of the field of view and images were reconstructed using a 6mm FWHM Hanning filter. A simulated [^{11}C]SCH 23390 data set was generated using a measured plasma input function and a two tissue compartmental model to simulate regional tissue kinetics using rate constants for different brain regions taken from human PET data, K_1 (0.08 to 0.13 ml plasma^{-1} min^{-1}), k_2 (0.24 to 0.37 min^{-1}), k_3 (0 to 0.14 min^{-1}), k_4 (0.1 min^{-1}) for 34 time frames (4x15s, 4x 30s, 7x60s, 5x120s ,14x300s). The cerebellum was simulated with a one tissue compartment model. Two dynamic data sets were generated; a noise free data set and the other consistent with an injection of 370MBq of activity. The two data sets were analysed with DEPICT to estimate parametric images of V_D and model order.

3.3 Measured Data Sets

Two measured data sets, which were taken from ongoing clinical studies (MRC Cyclotron Unit, Hammersmith Hospital, London U.K.), were analysed with DEPICT. Both data sets were acquired on the ECAT EXACT3D (CTI, Knoxville, TN) (Spinks et al., 2000). The data were reconstructed with model based scatter correction and measured attenuation correction using the method of filtered back projection (ramp filter, 0.5 Ny). The reconstructed images had a resolution of 4.8 x 4.8 x 5.6 mm at the centre of the field of view :

^{11}C Diprenorphine (opiate receptor): 130 MBq of the radioligand was injected into a normal male volunteer and acquisition consisted of 32 temporal frames of data (1x50s, 3x10s, 7x30s, 12x120s, 6x300s, 3x600s). Continuous arterial sampling and metabolite analyses were performed during the scan which allowed for the generation of a metabolite corrected plasma input function as described previously (Jones et al., 1994). DEPICT was used to estimate parametric images of V_D and model order using a plasma input analysis.

^{11}C WAY-100635 (5-HT$_{1A}$ receptor): 243 MBq of the radioligand was injected into a normal male volunteer and acquisition consisted of 22 temporal frames of data (1x15s, 3x5s, 2x15s, 4x60s,

7x300s, 5x600s). A region of interest was defined on the cerebellum for the extraction of a reference region TAC. DEPICT was used to estimate parametric images of $BP.f_2$ and model order using a reference tissue input analysis.

4 Results

4.1 1D Simulations

A summary of the results from the 1D noise simulations are presented in Figure 7 for the plasma input model. DEPICT was able to obtain a good fit to the data. Both DEPICT and spectral analysis performed well in terms of parameter and model order estimation. Table 2 shows that DEPICT produces the lowest Mean Square Error (MSE) of the three methods. The reference tissue input

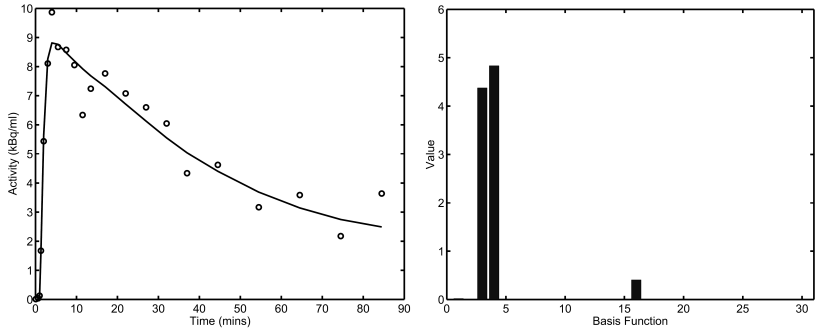

(a) Example DEPICT fit (b) DEPICT spectrum from fit in (a)

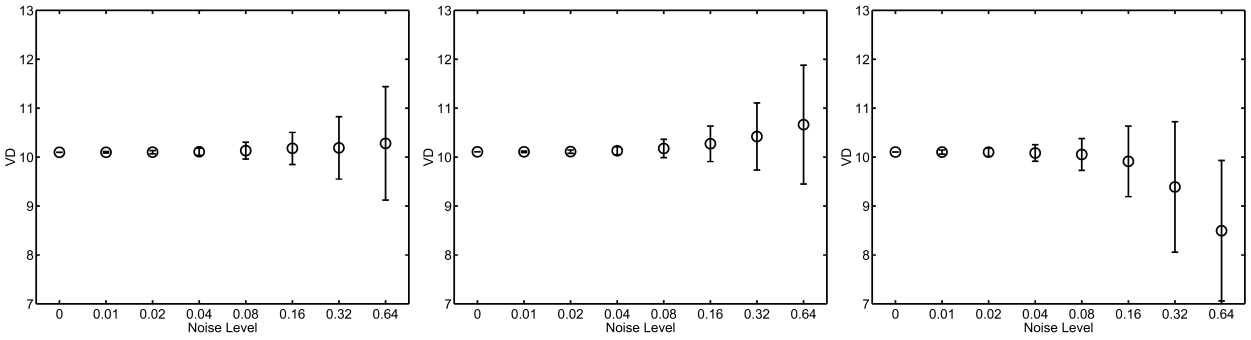

(c) DEPICT V_D (d) Spectral analysis V_D (e) Logan analysis V_D

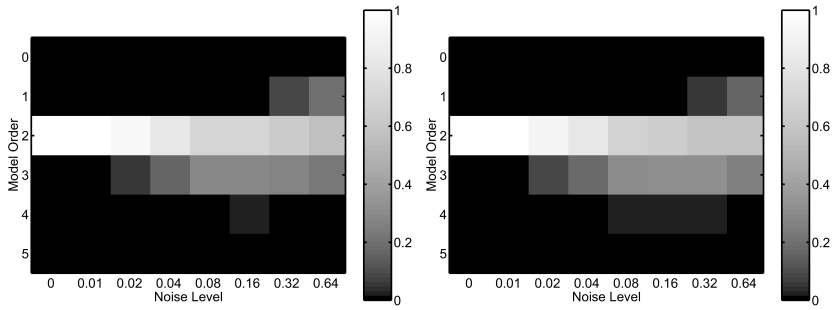

(f) DEPICT Model Order (g) Spectral analysis Model Order

FIGURE 7: 1D Simulation: Plasma Analysis. In subfigures (f) and (g) the colour bar indicates the fraction of fits which corresponded to a particular model order.

simulations are summarised in Figure 8 and Table 3. Again DEPICT obtained a good fit to the data and a reasonable model order estimation. Table 3 shows that DEPICT produces the lowest Mean Square Error (MSE) of the two methods.

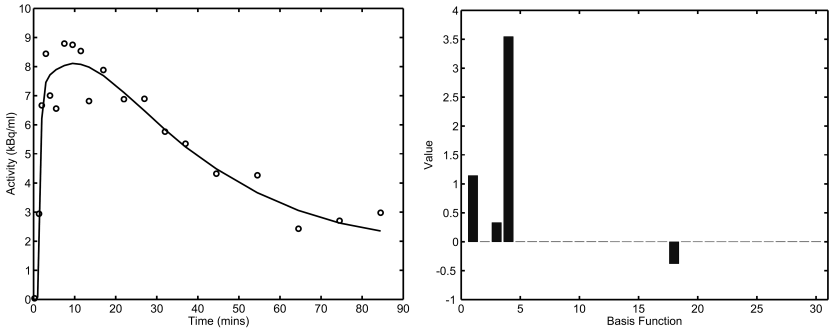

(a) Example DEPICT fit

(b) DEPICT spectrum from fit in (a)

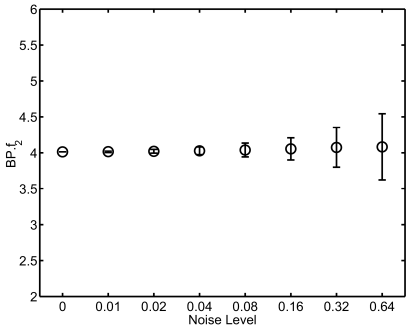

(c) DEPICT $BP.f_2$

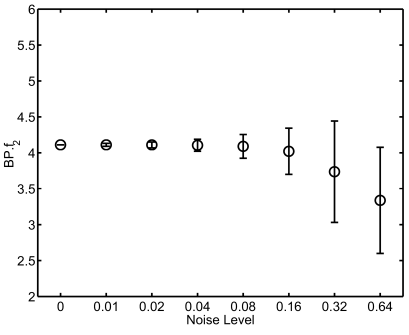

(d) Logan analysis $BP.f_2$

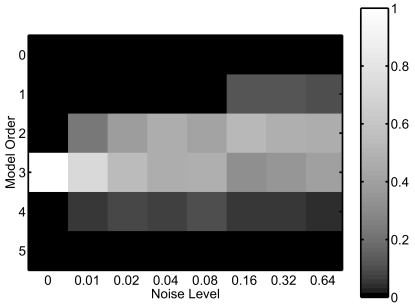

(e) DEPICT Model Order

FIGURE 8: 1D Simulation: Reference Tissue Analysis. In subfigure (e) the colour bar indicates the fraction of fits which corresponded to a particular model order.

4.2 4D Simulations

Parametric images estimated from the noisy 4D realisation using DEPICT were of good quality and are presented in Figure 9. DEPICT accurately estimates the number of tissue compartments used in the simulation, (see Figure 9b), with two tissue compartments estimated on average within the cortical regions and one tissue compartment on average within the cerebellum. The regularization parameter was calculated as $\hat{\mu} = 0.045$ (see Figure 10(a)). DEPICT was also applied to the noise free data set and this allowed for the calculation of the percentage error in the V_D estimate. The error distribution is given in Figure 10(b).

Noise Level		0	0.01	0.02	0.04	0.08	0.16	0.32	0.64
DEPICT	$\hat{\mu}$	0.0001	0.0100	0.0120	0.0138	0.0328	0.0482	0.1990	0.4190
	MSE	0.0002	0.0004	0.0011	0.0036	0.0107	0.0267	0.0815	0.2190
Logan analysis	MSE	0.0123	0.0127	0.0137	0.0180	0.0356	0.1040	0.5670	0.9840
Spectral analysis	MSE	0.0089	0.0089	0.0093	0.0103	0.0149	0.0325	0.0942	0.2280

TABLE 2: 1D Simulation: Summary Parameters for V_D estimation with a plasma input function. Mean Squared Error (MSE), Regularization Parameter $\hat{\mu}$.

Noise Level		0	0.01	0.02	0.04	0.08	0.16	0.32	0.64
DEPICT	$\hat{\mu}$	0.0001	0.0010	0.0014	0.0026	0.0056	0.0187	0.0414	0.0869
	MSE	0.0077	0.0081	0.0085	0.0155	0.0356	0.1060	0.2790	0.8180
Logan analysis	MSE	0.0108	0.0128	0.0167	0.0345	0.1230	0.4040	1.7400	4.1400

TABLE 3: 1D Simulation: Summary Parameters for $BP.f_2$ estimation with a reference tissue input function. Mean Squared Error (MSE), Regularization Parameter $\hat{\mu}$.

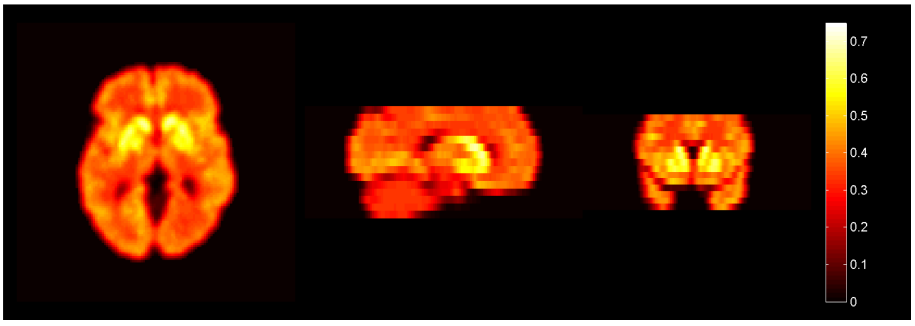

(a) V_D image

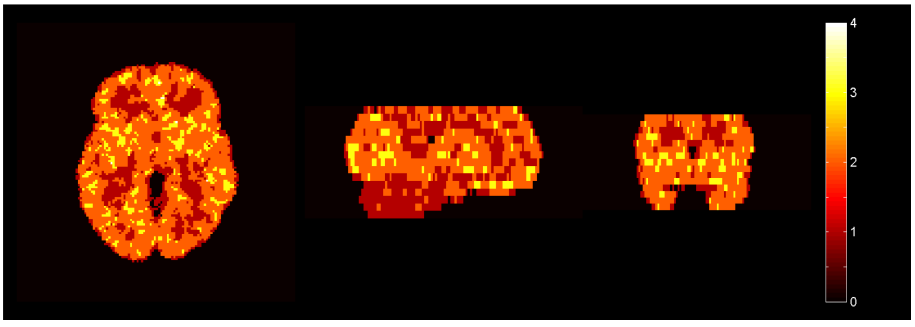

(b) Model Order image

FIGURE 9: 4D Simulation: Parametric images estimated using DEPICT.

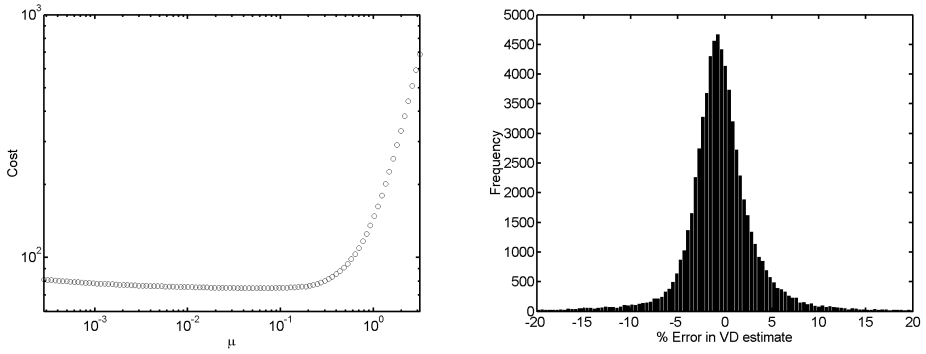

(a) Cost function for regularization parameter (μ) (b) % Error of V_D estimate shown in Figure 9

FIGURE 10: 4D Simulation: Cost function and error in V_D estimate.

4.3 Measured Data

Both the parametric images of V_D for [^{11}C]diprenorphine and $BP.f_2$ for [^{11}C]WAY-100635 were of good quality and reflected the known distribution of opiate and 5-HT$_{1A}$ receptor sites respectively. The model order images for both radioligands showed less structure than the 4D simulation but both reflected the model order expected for [^{11}C]diprenorphine (Jones et al., 1994) and [^{11}C]WAY-100635 (Gunn et al., 1998; Farde et al., 1998; Parsey et al., 2000). These parametric images took 1 hour to compute with DEPICT on a desktop workstation (equivalent computation times for parametric images generated by the Logan analysis and Spectral analysis would be 5 mins and 30 mins respectively). The regularization parameters were calculated as $\hat{\mu} = 0.0095$ for [^{11}C]diprenorphine and $\hat{\mu} = 0.015$ for [^{11}C]WAY-100635 (see Figure 12).

5 Discussion

The current paper has introduced, DEPICT, a tracer kinetic modelling technique for the quantitative analysis of dynamic *in vivo* radiotracer studies which allows for the data-driven estimation of parametric images based on compartmental theory. DEPICT requires no *a priori* decision about the tracers fate *in vivo*, instead determining the most appropriate model from the information contained within the data. Although, the method is classed as data-driven it is founded on compartmental theory (Gunn et al., 2001) and this enables parameter estimates to be interpreted within a traditional compartmental framework. The system macro parameters are simply determined from the estimated IRF. The method can be applied to dynamic radiotracer studies involving either a bolus or bolus-infusion tracer administration scheme. DEPICT is general, and whilst the examples here are concerned with tracers exhibiting reversible kinetics, the method is equally applicable to systems with irreversible kinetics. In addition to parameter estimates, DEPICT returns model order estimates which correspond to the number of numerically identifiable compartments in the system. There may be additional compartments that are not supported by the statistical quality of the data, however this is not in any way a practical restriction.

DEPICT uses a basis function approach (Koeppe et al., 1985; Cunningham and Jones, 1993; Gunn et al., 1997) to the parameter estimation problem. The constructed problem is ill-posed and its solution requires an appropriate constraint. Whilst, spectral analysis approaches this problem using the non-negative least squares algorithm (Cunningham and Jones, 1993), DEPICT employs the method of basis

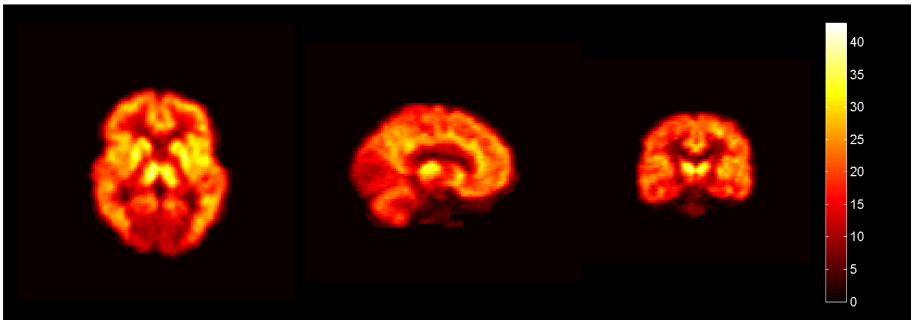

(a) [^{11}C]Diprenorphine: V_D image

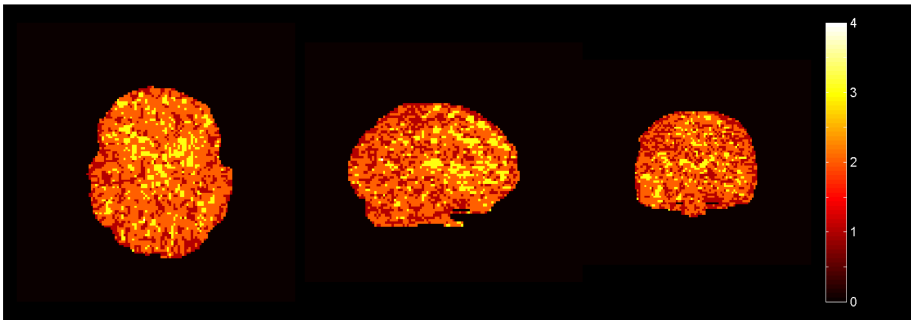

(b) [^{11}C]Diprenorphine: Model Order image

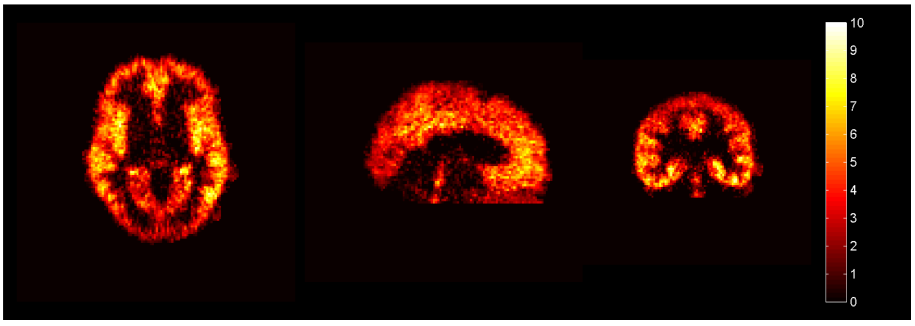

(c) [^{11}C]WAY-100635: $BP.f_2$ image

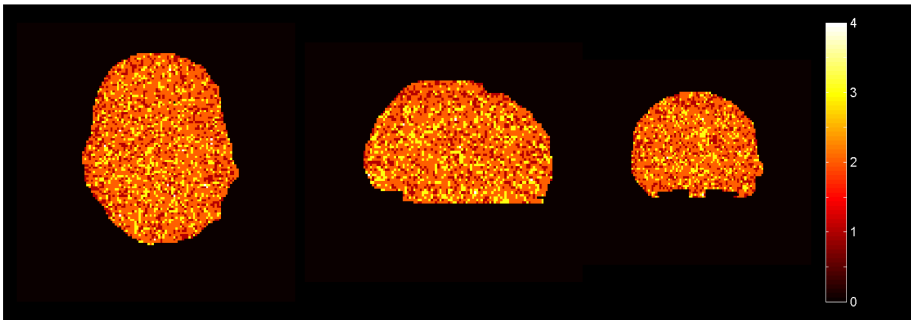

(d) [^{11}C]WAY-100635: Model Order image

FIGURE 11: Measured data: Parametric images estimated using DEPICT.

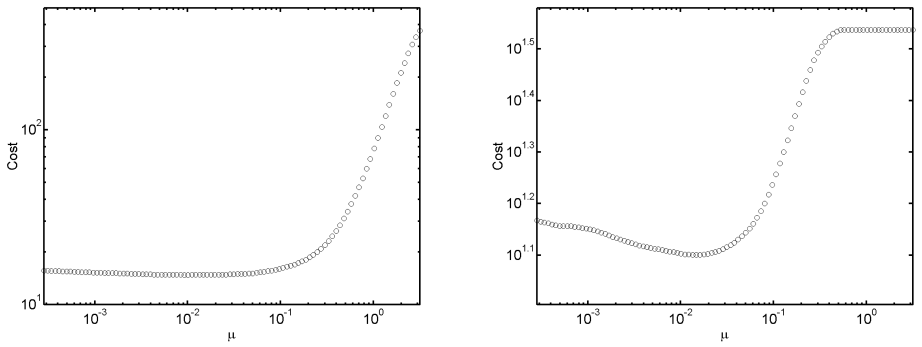

(a) [^{11}C]Diprenorphine (b) [^{11}C]WAY-100635

FIGURE 12: Measured data: Cost functions for regularization parameter (μ).

pursuit denoising (Chen, 1995) which involves a 1-norm penalty function on the coefficients. Both methods lead to a sparse solution but DEPICT does not constrain the coefficients to be positive which makes it appropriate for application to the general reference tissue model. Basis pursuit denoising is a technique that extracts a subset of terms from an overcomplete dictionary and thus it is possible to provide a model which is interpretable, whilst retaining good approximating capability. The principle behind the approach is to trade off the error in approximation with the sparseness of the representation.

The three data-driven methods investigated all performed well for low noise levels, as determined from the 1D simulations, with DEPICT returning the lowest mean squared error. The Logan analysis demonstrated a bias at higher noise levels which has been documented recently (Slifstein and Laruelle, 2000). To address the issue of noise induced bias in the Logan analysis two approaches have since been developed (Logan et al., 2001; Varga and Szabo, 2002). These modifications would have improved the performance of the Logan analysis at high noise levels but were not considered here as the aim was to introduce DEPICT and compare it against the data-driven methods in common use. DEPICT and spectral analysis allow for the estimation of the model order. The model order was well characterized by both methods for the 1D plasma input simulations and using DEPICT for the reference tissue input simulations. Spectral analysis is not valid for the general reference tissue model as it does not permit negative coefficients which can occur in the impulse response function.

In summary, this paper has introduced a new method, DEPICT, which delivers parametric images or regional parameter estimates from dynamic radiotracer imaging studies without the need to specify a compartmental structure. DEPICT is applicable to both plasma and reference tissue input analyses. The results presented demonstrate that DEPICT is highly competitive with existing *data-driven* estimation methods. Furthermore, DEPICT is a transparent data-driven modelling approach as it returns, not only macro parameter values, but also information on the underlying model structure.

A Logan Plot derivation

Here, a formal derivation of the Logan plot is presented for both a plasma and reference tissue input function. The plasma input Logan plot corresponds to the original presentation by Logan et al. (1990). The reference tissue input analysis presented here differs from Logan et al. (1996) in that it proves that the plot is valid for an arbitrary number of compartments in the reference tissue as well as the target tissue. Both derivations presented exclude the presence of vascular contribution to the tissue signal.

A.1 Plasma Input

The Logan plot with a plasma input (Logan et al., 1990) is given by,

$$\frac{\int_0^t C_T(t)dt}{C_T(t)} \simeq V_D \frac{\int_0^t C_P(t)dt}{C_T(t)} + c. \tag{24}$$

From Gunn et al. (2001) the general expression for the target tissue is given by,

$$C_T(t) = \sum_{i=1}^{n} \phi_i e^{-\theta_i t} \otimes C_P(t), \tag{25}$$

and the volume of distribution by,

$$V_D = \sum_{i=1}^{n} \frac{\phi_i}{\theta_i}. \tag{26}$$

Without loss of generality an ordering on the θ's is imposed such that $\theta_1 > \theta_2 > \ldots > \theta_n$. Substituting equation (25) into the left hand side of equation (24) yields,

$$\begin{aligned}
\frac{\int_0^t C_T(t)dt}{C_T(t)} &= \frac{\int_0^t \sum_{i=1}^n \phi_i e^{-\theta_i t} \otimes C_P(t)dt}{C_T(t)}, && (27)\\
&= \frac{\sum_{i=1}^n \frac{\phi_i}{\theta_i}(1 - e^{-\theta_i t}) \otimes C_P(t)}{C_T(t)}, && (28)\\
&= \frac{\sum_{i=1}^n \frac{\phi_i}{\theta_i} \otimes C_P(t)}{C_T(t)} - \frac{\sum_{i=1}^n \frac{\phi_i}{\theta_i} e^{-\theta_i t} \otimes C_P(t)}{C_T(t)}, && (29)\\
&= \sum_{i=1}^{n} \frac{\phi_i}{\theta_i} \frac{\int_0^t C_P(t)dt}{C_T(t)} - \frac{\sum_{i=1}^n \frac{\phi_i}{\theta_i} e^{-\theta_i t} \otimes C_P(t)}{C_T(t)}, && (30)\\
&= V_D \frac{\int_0^t C_P(t)}{C_T(t)} - \frac{\sum_{i=1}^n \frac{\phi_i}{\theta_i} e^{-\theta_i t} \otimes C_P(t)}{\sum_{i=1}^n \phi_i e^{-\theta_i t} \otimes C_P(t)}. && (31)
\end{aligned}$$

For suitably large t,

$$\frac{\int_0^t C_T(t)dt}{C_T(t)} \simeq V_D \frac{\int_0^t C_P(t)dt}{C_T(t)} - \frac{1}{\theta_n}. \tag{32}$$

A.2 Reference Tissue Input

The Logan plot with a reference tissue input (Logan et al., 1996) is given by,

$$\frac{\int_0^t C_T(t)dt}{C_T(t)} \simeq \frac{V_D}{V_D'}\frac{\int_0^t C_R(t)dt}{C_T(t)} + c. \tag{33}$$

From Gunn et al. (2001) the general expression for the target tissue is given by,

$$C_T(t) = \phi_0\delta(t) + \sum_{i=1}^{m+n-1} \phi_i e^{-\theta_i t} \otimes C_R(t), \tag{34}$$

and the volume of distribution ratio by,

$$\frac{V_D}{V_D'} = \phi_0 + \sum_{i=1}^{m+n-1} \frac{\phi_i}{\theta_i}. \tag{35}$$

Without loss of generality an ordering on the θ's is imposed such that $\theta_1 > \theta_2 > \ldots > \theta_{m+n-1}$.

Substituting equation (34) into the left hand side of equation (33) yields,

$$\begin{aligned}
\frac{\int_0^t C_T(t)dt}{C_T(t)} &= \frac{\int_0^t (\phi_0\delta(t) + \sum_{i=1}^{m+n-1} \phi_i e^{-\theta_i t}) \otimes C_R(t)dt}{C_T(t)}, && (36)\\
&= \frac{\phi_0 \int_0^t C_R(t)dt + \sum_{i=1}^{m+n-1} \frac{\phi_i}{\theta_i} \int_0^t C_R(t)dt}{C_T(t)} - \frac{\sum_{i=1}^{m+n-1} \frac{\phi_i}{\theta_i} e^{-\theta_i t} \otimes C_R(t)}{C_T(t)}, && (37)\\
&= \frac{\left(\phi_0 + \sum_{i=1}^{m+n-1} \frac{\phi_i}{\theta_i}\right) \otimes C_R(t)}{C_T(t)} - \frac{\sum_{i=1}^{m+n-1} \frac{\phi_i}{\theta_i} e^{-\theta_i t} \otimes C_R(t)}{C_T(t)}, && (38)\\
&= \left(\phi_0 + \sum_{i=1}^{m+n-1} \frac{\phi_i}{\theta_i}\right) \frac{\int_0^t C_R(t)dt}{C_T(t)} - \frac{\sum_{i=1}^{m+n-1} \frac{\phi_i}{\theta_i} e^{-\theta_i t} \otimes C_R(t)}{C_T(t)}, && (39)\\
&= \frac{V_D}{V_D'}\frac{\int_0^t C_R(t)dt}{C_T(t)} - \frac{\sum_{i=1}^{m+n-1} \frac{\phi_i}{\theta_i} e^{-\theta_i t} \otimes C_R(t)}{\phi_0\delta(t) + \sum_{i=1}^{m+n-1} \phi_i e^{-\theta_i t} \otimes C_R(t)}. && (40)
\end{aligned}$$

For suitably large t,

$$\frac{\int_0^t C_T(t)dt}{C_T(t)} \simeq \frac{V_D}{V_D'}\frac{\int_0^t C_R(t)dt}{C_T(t)} - \frac{1}{\theta_{m+n-1}}. \tag{41}$$

B Glossary

Symbol	Description	Units
$C_T(t)$	Concentration time course of radioactivity in the target tissue	$kBq.mL^{-1}$
$C_R(t)$	Concentration time course of radioactivity in the reference tissue	$kBq.mL^{-1}$
$C_P(t)$	Concentration time course of radioactivity in plasma	$kBq.mL^{-1}$
$C_B(t)$	Concentration time course of radioactivity in whole blood	$kBq.mL^{-1}$
$C_I(t)$	Concentration time course of radioactivity of the input function	$kBq.mL^{-1}$
$\boldsymbol{\phi}$	Parameter vector for coefficients of the general impulse response function	
$\boldsymbol{\theta}$	Parameter vector for exponents of the general impulse response function	
t_j^s	Start time for the jth temporal frame	min
t_j^e	End time for the jth temporal frame	min
n	Number of tissue compartments in the target tissue	
m	Number of tissue compartments in the reference tissue	
q	Number of exponential terms in the impulse response function	
$\boldsymbol{\Psi}$	Matrix of basis functions or "Dictionary"	$kBq.mL^{-1}$
$\mathbf{y}$	Measured PET tissue data	$kBq.mL^{-1}$
μ	Regularization parameter	
V_D	Volume of distribution of the target tissue	$(mL\,plasma).(mL\,tissue)^{-1}$
V_D'	Volume of distribution of the reference tissue	$(mL\,plasma).(mL\,tissue)^{-1}$
K_I	Irreversible uptake rate constant from plasma for the target tissue	$(mL\,plasma).min^{-1}.(mL\,tissue)^{-1}$
BP	Binding Potential	$(mL\,plasma).(mL\,tissue)^{-1}$
V_B	Fractional blood volume	
f_1	Plasma free fraction	
f_2	Tissue free fraction	
B_{max}	Maximum concentration of receptor sites	nM
$K_{D_{Tracer}}$	Equilibrium disassociation rate constant	nM
F_i	Free concentration of competing ligand	nM
K_{D_i}	Equilibrium disassociation rate constant of competing ligand	nM
$\otimes$	Convolution operator	

References

J. A. D. Aston, R. N. Gunn, K. J. Worsley, Y. Ma, A. C. Evans, and A. Dagher. A statistical method for the analysis of positron emission tomography neuroreceptor ligand data. *Neuroimage*, 12(3): 245–256, 2000.

G. Blomqvist, S. Pauli, L. Farde, L. Ericksson, A. Persson, and C. Halldin. *Clinical Research and Clinical Diagnosis (C. Beckers, A. Goffinet, and A. Bol, Eds)*, chapter : Dynamic models of reversible ligand binding, pages 35–44. Kluwer Academic Publishers, 1989.

R. E. Carson. *Positron emission tomography and autoradiography: Principles and applications for the brain and heart*, chapter 8: Parameter estimation in positron emission tomography, pages 347–90. Raven Press, New York, 1986.

R. E. Carson, S. C. Huang, and M. E. Green. Weighted integration method for local cerebral blood flow measurements with positron emission tomography. *J Cereb Blood Flow Metab*, 6:245–58., 1986.

S.S. Chen. *Basis Pursuit*. Ph.D. Thesis, Dept. of Statistics, Stanford University, 1995.

S.S. Chen, D.L. Donoho, and M.A. Saunders. Atomic decomposition by basis pursuit. *SIAM Journal on Scientific Computing*, 20(1):33–61, 1999.

V. J. Cunningham, S. P. Hume, G. R. Price, R. G. Ahier, J. E. Cremer, and A. K. Jones. Compartmental analysis of diprenorphine binding to opiate receptors in the rat in vivo and its comparison with equilibrium data in vitro. *J Cereb Blood Flow Metab*, 11(1):1–9, 1991.

V. J. Cunningham and T. Jones. Spectral analysis of dynamic pet studies. *J Cereb Blood Flow Metab*, 13(1):15–23., 1993.

V.J. Cunningham, R.N. Gunn, H. Byrne, and J.C. Matthews. *Quantitative functional brain imaging with positron emission tomography (Eds Carson RE, Daube-Witherspoon ME, Herscovitch P)*, chapter 49: Suppression of noise artefacts in spectral analysis of dynamic PET data, pages 329–337. Academic Press, 1998.

L. Farde, H. Ito, C.G. Swahn, V.W. Pike, and C. Halldin. Quantitative analyses of carbonyl-carbon-11-WAY-100635 binding to central 5-hydroxytryptamine-1A receptors in man. *J Nucl Med*, 39(11): 1965–71., 1998.

D. Feng, S. C. Huang, Z. Wang, and D. Ho. An unbiased parametric imaging algorithm for uniformly sampled biomedical system parameter estimation. *IEEE Trans Med Imag*, 15(4):512–18., 1996.

A. Gjedde. Calculation of cerebral glucose phosphorylation from brain uptake of glucose analogs in vivo: a re-examination. *Brain Res Rev*, 4:237–274, 1982.

R. N. Gunn, S. R. Gunn, and V. J. Cunningham. Positron emission tomography compartmental models. *J Cereb Blood Flow Metab*, 21(6):635–652, 2001.

R. N. Gunn, A. A. Lammertsma, S. P. Hume, and V. J. Cunningham. Parametric imaging of ligand-receptor binding in PET using a simplified reference region model. *NeuroImage*, 6(4):279–287, 1997.

R. N. Gunn, P. A. Sargent, C. J. Bench, E. A. Rabiner, S. Osman, V. W. Pike, S. P. Hume, P. M. Grasby, and A. A. Lammertsma. Tracer kinetic modeling of the 5-HT_{1A} receptor ligand [carbonyl-11C]WAY-100635 for PET. *Neuroimage*, 8(4):426–40, 1998.

J.S.U. Hjorth. *Computer Intensive Statistical Methods Validation, Model Selection, and Bootstrap.* Chapman & Hall, London, 1994.

S. C. Huang and M. E. Phelps. *Positron emission tomography and autoradiography: Principles and applications for the brain and heart*, chapter 7: Principles of tracer kinetic modeling in positron emission tomography and autoradiography, pages 287–346. Raven Press, New York, 1986.

S. P. Hume, R. Myers, P. M. Bloomfield, J. Opacka-Juffry, J. E. Cremer, R. G. Ahier, S. K. Luthra, D. J. Brooks, and A. A. Lammertsma. Quantitation of carbon-11-labeled raclopride in rat striatum using positron emission tomography. *Synapse*, 12:4754, 1992.

A.K. Jones, V.J. Cunningham, S.K. Ha-Kawa, T. Fujiwara, Q. Liyii, S.K. Luthra, J. Ashburner, S. Osman, and T. Jones. Quantitation of [11C]diprenorphine cerebral kinetics in man acquired by PET using presaturation, pulse-chase and tracer-only protocols. *J Neurosci Methods*, 51(2): 123–134, 1994.

S. S. Kety. The theory and application of the exchange of inert gases at the lungs and tissues. *Pharmacol Rev*, 3:1–41., 1951.

R. A. Koeppe, J. E. Holden, and W. R. Ip. Performance comparison of parameter estimation techniques for the quantitation of local cerebral blood flow by dynamic positron computed tomography. *J Cereb Blood Flow Metab*, 5:224–34., 1985.

A. A. Lammertsma, C. J. Bench, S. P. Hume, S. Osman, K. Gunn, D. J. Brooks, and R. S. Frackowiak. Comparison of methods for analysis of clinical [11C]raclopride studies. *J Cereb Blood Flow Metab*, 16(1):42–52, 1996.

A. A. Lammertsma and S. P. Hume. Simplified reference tissue model for PET receptor studies. *NeuroImage*, 4:153–8, 1996.

M. Laruelle. Imaging synaptic neurotransmission with *in vivo* binding competition techniques: A critical review. *J Cereb Blood Flow Metab*, 20(3):423–51, 2000.

J. Logan, J. S. Fowler, N. D. Volkow, G-J. Wang, Y-S. Ding, and D. L. Alexoff. Distribution volume ratios without blood sampling from graphical analysis of pet data. *J Cereb Blood Flow Metab*, 18: 834840, 1996.

J. Logan, J. S. Fowler, N. D. Volkow, A. P. Wolf, S. L. Dewey, D. J. Schlyer, R. R. MacGregor, R. Hitzemann, B. Bendriem, S. J. Gatley, and D. R. Christman. Graphical analysis of reversible radioligand binding from time-activity measurements applied to [N-11C-methyl]-(-)-cocaine PET studies in human subjects. *J Cereb Blood Flow Metab*, 10(5):740–7, 1990.

J. Logan, J.S. Fowler, N.D. Volkow, Y.S. Ding, G.J. Wang, and D.L. Alexoff. A strategy for removing the bias in the graphical analysis method. *J Cereb Blood Flow Metab*, 21(3):307–320, 2001.

Y. Ma and A.C. Evans. Analytical modeling of PET imaging with correlated functional and structural images. *IEEE Trans Nucl Sci*, 44(6(2)):2439–44., 1997.

Y. Ma, M. Kamber, and A.C. Evans. 3d simulation of PET brain images using segmented MRI data and positron tomograph characteristics. *Comput Med Imaging Graph*, 17(4-5):365–71, 1993.

B.M. Mazoyer, R.H. Huesman, T.F. Budinger, and B.L. Knittel. Dynamic PET data analysis. *J Comput Assist Tomogr*, 10(4):645–653, 1986.

C. Mészáros. The BPMPD interior point solver for convex quadratic problems. Technical Report WP 98-8, Computer and Automation Research Institute, Hungarian Academy of Sciences, Budapest, 1998.

M. A. Mintun, M. E. Raichle, M. R. Kilbourn, G.F. Wooten, and M. J. Welch. A quantitative model for the in vivo assessment of drug binding sites with positron emission tomography. *Ann Neurol*, 15:217–227, 1984.

R. V. Parsey, M. Slifstein, D. R. Hwang, A. Abi-Dargham, N. Simpson, O. Mawlawi, N. N. Guo, R. Van Heertum, J. J. Mann, and M. Laruelle. Validation and reproducibility of measurement of 5-HT_{1A} receptor parameters with [carbonyl-11C]WAY-100635 in humans: comparison of arterial and reference tisssue input functions. *J Cereb Blood Flow Metab*, 20(7):1111–33, 2000.

C. S. Patlak and R. G. Blasberg. Graphical evaluation of blood-to-brain transfer constants from multiple-time uptake data. generalizations. *J Cereb Blood Flow Metab*, 5(4):584–90, 1985.

C. S. Patlak, R. G. Blasberg, and J. D. Fenstermacher. Graphical evaluation of blood-to-brain transfer constants from multiple-time uptake data. *J Cereb Blood Flow Metab*, 3(1):1–7, 1983.

M. E. Phelps, S. C. Huang, E. J. Hoffman, C. Selin, L. Sokoloff, and D. E. Kuhl. Tomographic measurement of local cerebral glucose metabolic rate in humans with (F-18)2-fluoro-2-deoxy-D-glucose: validation of method. *Ann Neurol*, 6(5):371–88, 1979.

K. Schmidt. Which linear compartmental systems can be analyzed by spectral analysis of PET output data summed over all compartments ? *J Cereb Blood Flow Metab*, 19:560–569, 1999.

J. Shao. Linear model selection by cross-validation. *J. of the American Statistical Association*, 88: 486–494, 1993.

M. Slifstein and M. Laruelle. Effects of statistical noise on graphic analysis of pet neuroreceptor studies. *J Nucl Med*, 41(12):2083–2088, 2000.

L. Sokoloff, M. Reivich, C. Kennedy, M. H. DesRosiers, C. S. Patlak, K. D. Pettigrew, O. Sakurada, and M. Shinohara. The 14C-deoxyglucose method for the measurement of local cerebral glucose utilisation: theory, procedure and normal values in the conscious and anaesthetized albino rat. *J Neurochem*, 28:897–916, 1977.

T.J. Spinks, T. Jones, P.M. Bloomfield, D.L. Bailey, M. Miller, D. Hogg, W.F. Jones, K. Vaigneur, J. Reed, J. Young, D. Newport, C. Moyers, M.E. Casey, and R. Nutt. Physical characteristics of the ECAT EXACT3D positron tomograph. *Phys Med Biol*, 45(9):2601–2618, 2000.

J. Varga and Z. Szabo. Modified regression model for the logan plot. *J Cereb Blood Flow Metab*, 22 (2):240–244, 2002.

H. Watabe, R. E. Carson, and H. Iida. The reference tissue model: Three compartments for the reference region. *NeuroImage*, 11(6):S12, 2000.